

# JGR Oceans

## RESEARCH ARTICLE

10.1029/2024JC021379

### Key Points:

- In the central Barents Sea, sea ice edge positions fluctuated in winter until the mid-2000s but have lately fixed along a warm current
- Since the mid-2000s, sea ice edges have been frequently identified along the continental slope in the northern Barents Sea in winter
- Until 2006, sea ice edges in the Greenland Sea were located at the East Greenland Current, but they shifted far west after 2006 in summer

### Supporting Information:

Supporting Information may be found in the online version of this article.

### Correspondence to:

R. Masunaga,  
masunagar@jamstec.go.jp

### Citation:

Masunaga, R., Komuro, Y., Kawasaki, T., & Ono, J. (2024). Observations of sea ice edge position in the Barents and Greenland Seas: Temporal variability and long-term changes. *Journal of Geophysical Research: Oceans*, 129, e2024JC021379. <https://doi.org/10.1029/2024JC021379>

Received 26 MAY 2024

Accepted 19 OCT 2024

### Author Contributions:

**Conceptualization:** R. Masunaga, Y. Komuro, T. Kawasaki, J. Ono

**Data curation:** R. Masunaga

**Formal analysis:** R. Masunaga

**Funding acquisition:** R. Masunaga, Y. Komuro

**Methodology:** R. Masunaga, Y. Komuro, T. Kawasaki, J. Ono

**Validation:** R. Masunaga

**Visualization:** R. Masunaga

**Writing – original draft:** R. Masunaga

**Writing – review & editing:**

R. Masunaga, Y. Komuro, T. Kawasaki, J. Ono

## Observations of Sea Ice Edge Position in the Barents and Greenland Seas: Temporal Variability and Long-Term Changes

R. Masunaga<sup>1</sup> , Y. Komuro<sup>1</sup> , T. Kawasaki<sup>2</sup> , and J. Ono<sup>3</sup> 

<sup>1</sup>Japan Agency for Marine-Earth Science and Technology, Yokohama, Japan, <sup>2</sup>Atmosphere and Ocean Research Institute, The University of Tokyo, Kashiwa, Japan, <sup>3</sup>National Institute of Polar Research, Tachikawa, Japan

**Abstract** Sea ice edges play an essential role in the Earth's climate and weather systems through active atmosphere-ice-ocean interactions. However, our understanding of the observed positions of sea ice edges remains limited. The present study investigated, on seasonal and longer timescales from 1979 to 2023, the variability in sea ice edge positions in the Barents and Greenland Seas. We objectively derived the positions of sea ice edges based on satellite-derived sea ice concentration gridded on a 25-km resolution. In the Barents Sea, warm, narrow currents flow eastward along the northern and southern rims of the Central Bank. Until the mid-2000s, sea ice edges fluctuated between these currents interannually during December–June, depending on the surface wind direction. However, after the mid-2000s, the sea ice edges were mostly positioned near the northern current or farther to the north. Furthermore, sea ice edges during October–March were identified frequently near the warm current flowing along the continental slope in the northern Barents Sea after the mid-2000s. In the Greenland Sea, sea ice edges were typically positioned near the East Greenland Current (EGC) throughout the year until 2006. However, sea ice edges in summer were located far to the west of the EGC after 2006. These observations suggest that the geographical relationship between sea ice edges and ocean currents has changed due to global warming.

**Plain Language Summary** Sea ice edges in the Arctic play an important role in the Earth's climate system. They can strengthen atmospheric cyclones and vertical motion in the atmosphere and the ocean in the Arctic by inducing intense heat and moisture releases from the ocean to the atmosphere. Furthermore, they could exert distinct impacts on global-scale atmosphere and ocean circulations. Therefore, a deeper understanding of the geographical positions of sea ice edges is essential for elucidating the climate system. This study investigated the sea ice edge positions in the Barents and Greenland Seas using satellite observations from 1979 to 2023. Sea ice edges rapidly advance southward during winter. Until the mid-2000s, sea ice edges were frequently identified along warm ocean currents in the Barents and Greenland Seas because warm currents obstruct further sea ice edge advances. However, sea ice edges have shifted far to the north of warm ocean currents after the mid-2000s in association with the recent shrinking in sea ice extent due to global warming. The change in sea ice edge positions might have affected the atmosphere and ocean circulations globally, which should be addressed in future studies.

### 1. Introduction

Sea ice plays an important role in the Earth's climate and weather systems as it inhibits the active exchange of heat, moisture, and momentum between the ocean and the atmosphere. Its high albedo reduces the net solar energy absorbed at the Earth's surface. Atmosphere-ice-ocean interactions are particularly active near marginal ice zones (Dumont, 2022). In particular, intense surface heat fluxes are induced on the open-water side of sea ice edges (Papritz & Spengler, 2017; Spensberger & Spengler, 2021).

The impacts of sea ice edge variability on the atmosphere and ocean circulation have been actively investigated in the Barents and Greenland Seas. The intensified heat fluxes can yield the frequent generation of polar lows (Kolstad, 2006, 2011; Landgren et al., 2019) and modulate the activity of synoptic-scale cyclones by affecting surface baroclinicity (Hoskins & Valdes, 1990; Inoue et al., 2012). Våge et al. (2018) argued that the retreat of sea ice edges in the Greenland Sea modified the properties of ocean water by triggering ocean convection. Furthermore, sea ice edge retreat resulted in a larger area of the open-water region, yielding a larger heat loss integrated over the Barents Sea (Årthun et al., 2012).

Thus, sea ice edges play a key role in climate and weather systems. Sea ice edge positions have been shifting poleward (Xia et al., 2014) in association with the decrease in the sea ice extent (Serreze et al., 2007; Stroeve et al., 2012). The trend and decadal-scale variation of sea ice edges were investigated using historical observations in the Barents and Greenland Seas during the mid-19th to 20th centuries (Divine & Dick, 2006) and using satellite-derived products over the entire Arctic in more recent years (Xia et al., 2014). In addition, extensive efforts have been made to improve the prediction skill of numerical models in determining sea ice edge positions (Dukhovskoy et al., 2015; Melsom et al., 2019).

However, our understanding of the observed positions of sea ice edges remains limited. The present study aims to investigate the variability in sea ice edge positions on seasonal and longer timescales using satellite observations. As previous studies have suggested that sea ice edges tended to be maintained near ocean currents in the Barents and Greenland Seas (Barton et al., 2018; Bitz et al., 2005; Wadhams, 1981), our primary objective is to describe the geographical relationship between the sea ice edges and surface ocean currents in these ocean regions and elucidate the changes in this relationship in recent decades.

The remainder of this paper is organized as follows. The data and sea ice edge detection methods are described in Section 2. The characteristics of sea ice edge positions in the Barents Sea are discussed in Section 3, and those in the Greenland Sea in Section 4. A discussion and summary are provided in Section 5 and Section 6, respectively.

## 2. Data and Methods

### 2.1. Data

We used the daily sea ice concentration estimated from passive microwave remote sensing provided by the National Snow and Ice Data Center (NSIDC) (DiGirolamo et al., 2022), which was estimated using the NASA Team algorithm (Cavalieri et al., 1997). This product is called the main sea ice product or NT in the present study. The daily fields were available with a 25-km resolution every other day from 1979 to 1987 and every day afterward until September 2023.

As sea ice distribution derived from microwave remote sensing tended to exhibit large errors near the sea ice edge (Meier, 2005; Meier et al., 2015), other sea ice products were used for verification. Specifically, the satellite-observed sea ice concentration derived using the bootstrap algorithm (BT) (Comiso, 2023), the U.S. National Ice Center Arctic Sea Ice Charts (NIC) (U.S. National Ice Center et al., 2006), and Multisensor Analyzed Sea Ice Extent (MASIE) (U.S. National Ice Center et al., 2010) were used. Analysts determined the NIC and MASIE sea ice distribution from multiple data sources. The NIC was available weekly from 1972 to 2007, and MASIE was available daily from 2006 to the present; hence, we combined these two products to create a continuous record since 1972 (NIC + MASIE). The detailed descriptions of the data processing are given in Text S1 in Supporting Information S1. We mostly used NT for our analysis, briefly discussing a comparison with BT and NIC + MASIE.

The Ocean Reanalysis System 5 (ORAS5) was used for the sea ice thickness, current components, and potential temperature (Copernicus Climate Change Service & Climate Data Store, 2021). The horizontal resolution of the Arctic region was approximately 9 km. The current components in the uppermost model layer were used as the surface fields. We confirmed that the sea ice edge distributions from ORAS5 and NT were generally consistent.

Daily satellite-derived sea ice motion data were obtained from the NSIDC with a 25-km resolution (Tschudi et al., 2019, 2020). For surface wind at a 10-m height and total surface heat fluxes, the monthly mean products of the ERA5 reanalysis were used on a  $0.25^\circ \times 0.25^\circ$  grid distribution (Hersbach et al., 2019, 2020). The ETOPO1 1 Arc-Minute Global Relief model was used for bathymetry (Amante & Eakins, 2009; NOAA National Geophysical Data Center, 2009).

These data were mostly analyzed from 1979 to 2023 when the satellite remote observations provided consistent sea ice records. They were re-gridded onto the Polar Stereographic projection with a 25-km resolution for plotting purposes.

### 2.2. Sea Ice Edge Detection

In recent studies, sea ice edge positions were commonly defined as 15% isolines of sea ice concentration (Dukhovskoy et al., 2015); thus, we followed this definition for consistency. The sea ice edge positions were

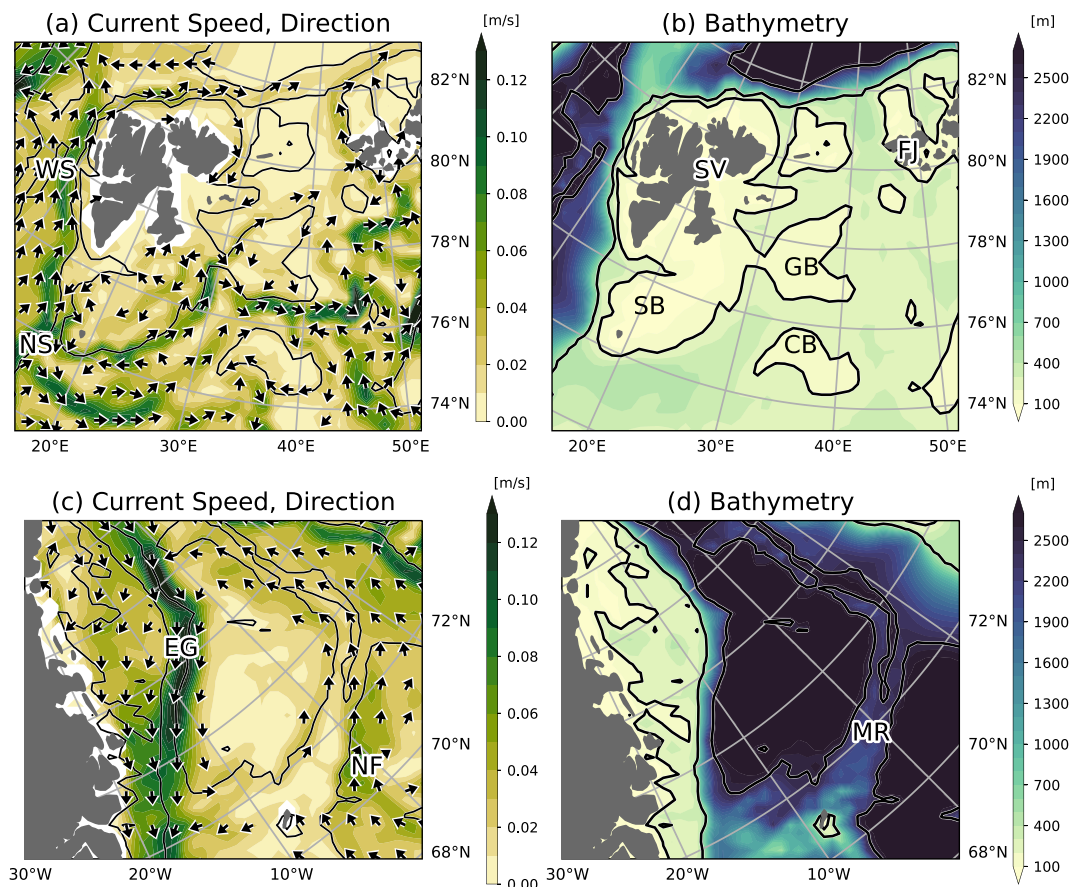


**Figure 1.** Annual climatology of surface ocean current speed ( $\text{m s}^{-1}$ ; shaded) and direction (arrows; indicated when the corresponding speed is  $0.015 \text{ m s}^{-1}$  or greater) averaged from November 1979 to October 2023 in the (a) Barents Sea and (c) Greenland Sea. Bathymetry measured as the downward depth (m; shaded) in the (b) Barents Sea and (d) Greenland Sea. The isolines of bathymetry for 200, 500, and 2,500 m are highlighted with contours. NS, Norwegian Atlantic Slope Current; WS, West Spitsbergen Current; SV, Svalbard; SB, Spitsbergen Bank; GB, Great Bank; CB, Central Bank; FJ, Franz Josef Land; MR, Mohns Ridge; EG, East Greenland Current; NF, Norwegian Atlantic Front Current.

determined from daily sea ice concentration. First, a target domain was classified into sea ice or open-water regions daily with a threshold of 15% sea ice concentration. Then, the sea ice grid cells in contact with the open-water grids were marked as sea ice edge grids (indicated with the dots in Figure S1 in Supporting Information S1). Thus, a daily sea ice edge distribution was obtained as a gridded field. Horizontal maps of sea ice edge occurrences were constructed from the daily gridded sea ice edge data by counting the number of sea ice edge grid emergences at each grid cell and dividing by the number of observations over a target period.

### 3. Variability in Sea Ice Edge Positions in the Barents Sea

Figure 1a shows the annual climatology of surface ocean currents in the study area. Part of the Norwegian Atlantic Slope Current bifurcates into the Barents Sea. The bifurcated currents mostly flow northeastward and follow the relatively deep troughs among the shallow banks (Figure 1b) (Eriksen et al., 2018). In particular, a narrow eastward current is located between the Central Bank (CB) and Great Bank (GB). Although less pronounced, another narrow current flows along the southwestern rim of the CB. The seasonality of these currents is indistinct. To the north of the Barents Sea, part of the West Spitsbergen Current turns clockwise around Svalbard and flows eastward along the continental slope as consistent with the simplified model (Nøst & Isachsen, 2003). The eastward current can be identified from August through April.

### 3.1. Seasonal Evolution and Long-Term Changes

To investigate long-term changes, the entire analysis period was divided into three segments: 1980–1993 (14 years), 1994–2008 (15 years), and 2009–2023 (15 years). Figure 2 shows each segment's sea ice edge occurrences for October, January, April, and July. The sea ice edge occurrences in the other months were similar to those in the adjacent months (figures omitted).

In a typical seasonal evolution, the sea ice edges were located at the northernmost positions in September. In 1979–1992/1980–1993 and 1993–2007/1994–2008 (first and second columns in Figure 2, respectively), the edges advanced southward from September to October (Figures 2a and 2b) and were located along the narrow warm current between the CB and GB during November–April (Figures 2d and 2e for January and Figures 2g and 2h for April), as described by Barton et al. (2018). From December to April, the edges advanced slightly and sometimes reached the south of the CB. The sea ice edges tended to avoid the CB; thus, a bimodal structure was straddled across the CB during this period. The sea ice edges started retreating in May and were distributed broadly in June–August (Figures 2j and 2k for July).

The sea ice edge distributions in 2008–2022/2009–2023 (third column in Figure 2) were distinct from those in the previous periods. In October–December, edges were frequently positioned along the continental slope in the northern Barents Sea (Figure 2c for October). Although the edges typically reached the trough between the CB and GB in January–April, they rarely reached the south of the CB (Figures 2f and 2i). Furthermore, to the northeast of Svalbard, high sea ice edge occurrence extended eastward along the continental slope in January–March for 2009–2023 compared with the previous periods (Figures 2d–2f for January).

The BT, NIC, and MASIE exhibited consistent features as the NT (Figure S2 in Supporting Information S1 for January as a typical example). In subsequent analysis, we focused on three features: the bimodal structure near the CB, frequent sea ice edge occurrence near the continental slope in October, and the eastward extension of sea ice edges to the northeast of Svalbard in January. These features would highlight the relationship between the sea ice edges and ocean currents.

### 3.2. Bimodal Structure Near the CB During December–May

The bimodal structure near the CB was further investigated by constructing histograms of sea ice edge positions near the CB in December–May. As described in Text S2 of Supporting Information S1, the daily edge positions were obtained for the green rectangular box in Figure S1a of Supporting Information S1, and the histograms were constructed for each year (shaded in Figure 3a). Although the rectangular box covers a large latitudinal domain to encompass all the daily sea ice edges, the latitudinal range shown in Figure 3a is limited to an area near the CB (rectangular box in Figure 2d). Each year, the sea ice edge position that occurred the most frequently (i.e., the mode) was considered typical positions.

The histogram modes (black line in Figure 3a) fluctuated between approximately 76.5°N and 74.5°N (upper and lower gray dashed lines in Figure 3a, respectively) from 1983 to 2004. The modes were located near 76.5°N (74.5°N) when the surface wind was northward (southward) (shaded in Figure 3b). Although the modes were sometimes located near 76.5°N even under the southward wind, such as in 1998, the secondary peaks of the histograms were located near 74.5°N (shaded in Figure 3a). Thus, seasonal-scale surface winds appeared to play a significant role in the interannual sea ice edge variability until 2004. However, the edges were anchored near 76.5°N from 2005 onward (Barton et al., 2018), regardless of the occasional southward wind. The modulation was associated with the sudden warming of ocean temperature (Figure 3c) (Skagseth et al., 2020). Furthermore, the sea ice thickness averaged for 2005–2023 was thinner than that averaged for 1986–2004 at the 95% confidence level (Figure 3d). Thinner sea ice should be less likely to reach the southern rim of the CB (i.e., 74.5°N) by sea ice transport crossing the warm current between the CB and GB. Thus, the sudden modulation of the sea ice edge variability is likely related to the sudden ocean warming and the associated sea ice thinning. We confirmed that the BT and NIC + MASIE yielded consistent features (Figure S3 in Supporting Information S1); thus, these results were insensitive to the selection of data products.

### 3.3. Sea Ice Edge Along the Continental Slope in October

Histograms were constructed to elucidate the variability in the sea ice edge positions in October (shaded in Figure 4a) for the green box indicated in Figure 2a (see Text S2 in Supporting Information S1 for details). The

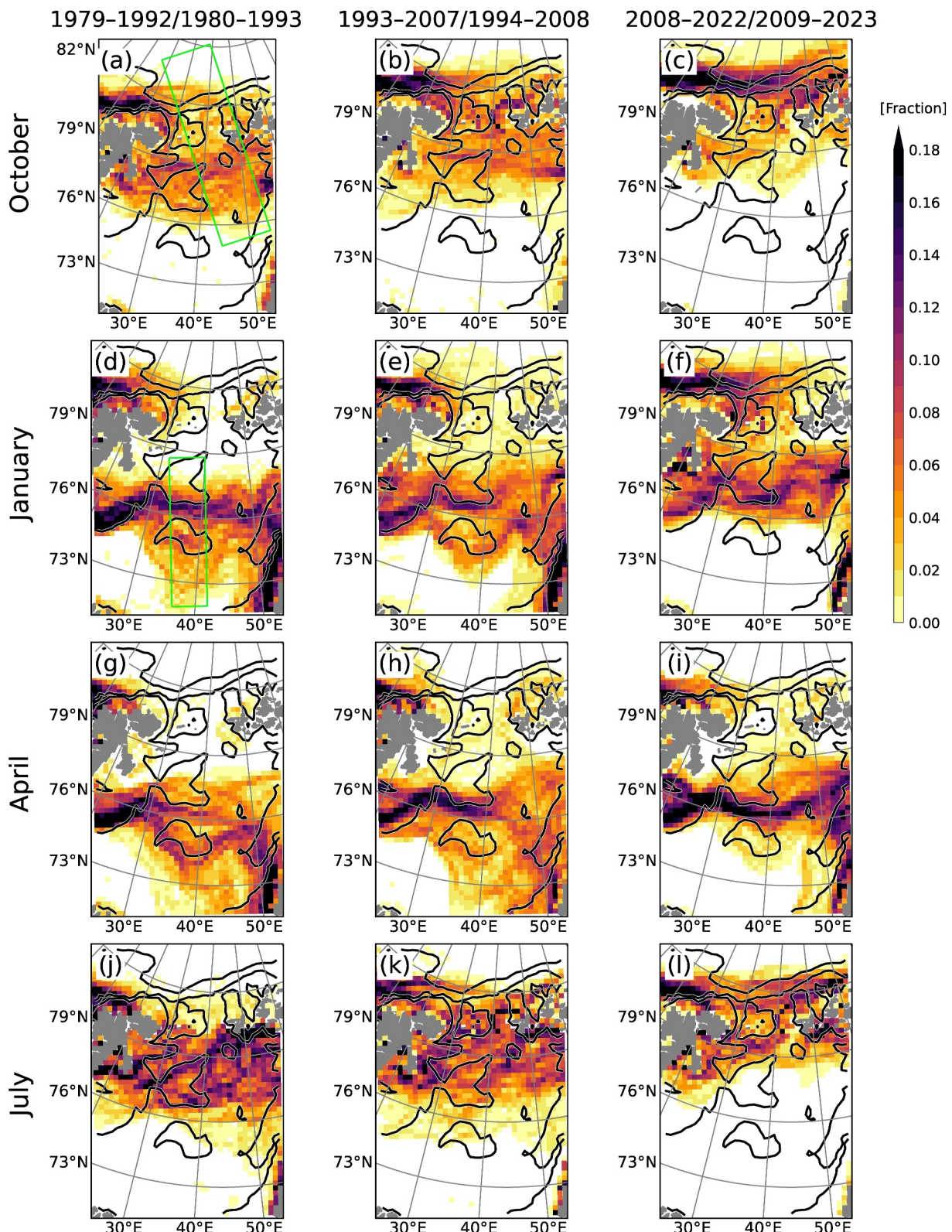


**Figure 2.** Sea ice edge occurrences at each grid cell based on NT accumulated over (a) 1979–1992, (b) 1993–2007, and (c) 2008–2022 in October, and (d, g, and j) 1980–1993 (e, h, and k) 1994–2008, and (f, i, and l) 2009–2023 in January, April, and July, respectively. The isolines of bathymetry for 200, 500, and 2,500 m are indicated with the contours. The rectangular boxes in panels (a, d) indicate the target domains for constructing the Hovmöller diagrams shown in Figures 4 and 3, respectively.

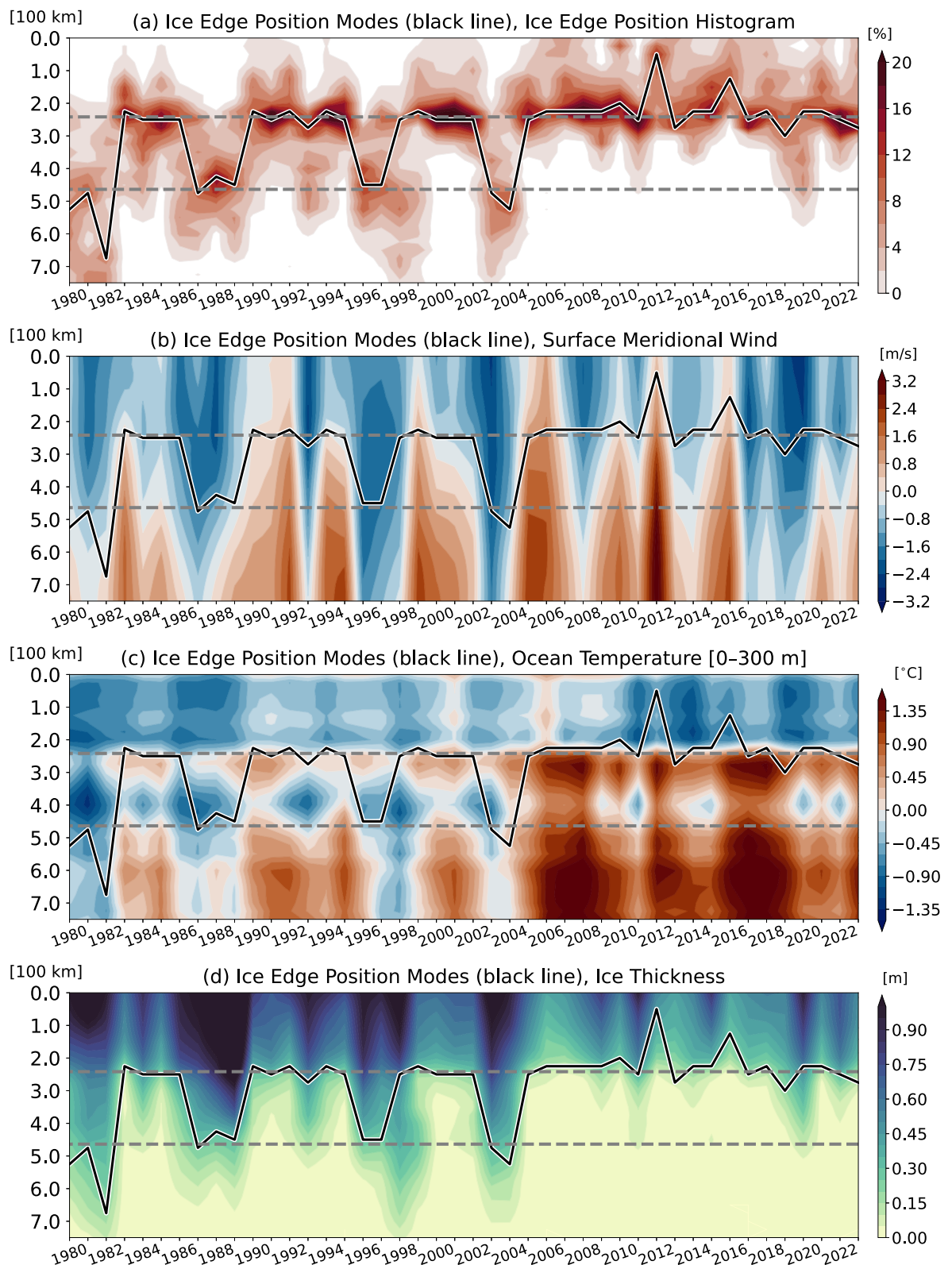
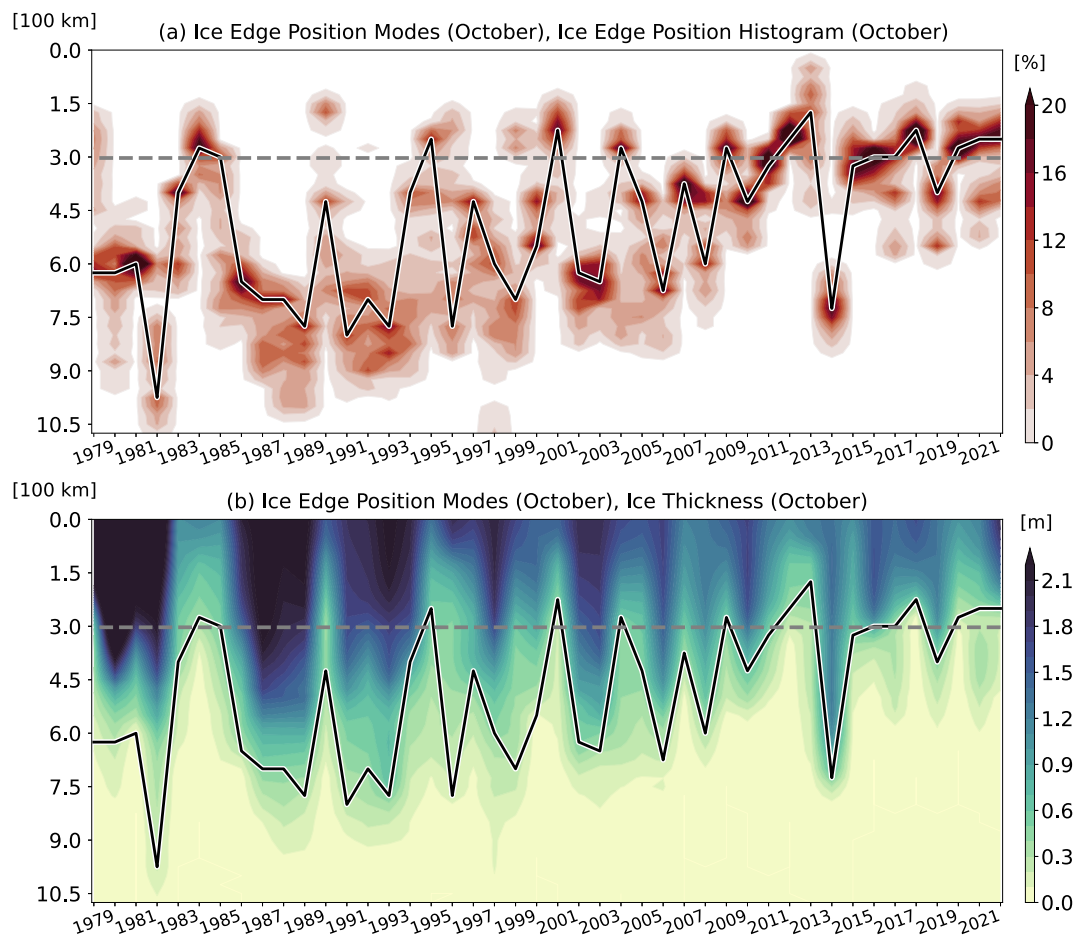


Figure 3.



**Figure 4.** (a) Sea ice edge position histograms based on NT (shaded; %) and (b) Hovmöller diagram of sea ice thickness in October (shaded; m) obtained for the reference box shown in Figure 2a. The modes of the sea ice edge position histograms are indicated with black lines. The dashed gray lines indicate 82°N.

modes (black line) were located near the continental slope (gray line) occasionally before 2008 but constantly in the subsequent period, except for 2014. This feature was consistent with the high sea ice edge occurrences confined to the continental slope in the most recent period (Figure 2c). The warm current along the continental slope (Figure 1a) appeared to obstruct the southward edge advance.

This feature was further elucidated by investigating the sea ice thickness (Figure 4b) and surface winds. The sea ice thickness was significantly thinner when the modes were located north of 82°N (13 years) than when located south of 80°N (19 years) with a 95% confidence level. This result was insensitive to the threshold for the edge positions. Thus, the high sea ice edge occurrence near the continental slope in the most recent period can be partly attributed to the decrease in typical sea ice thickness after 2008 (Figure 4b). Meanwhile, the correlation ( $r$ ) between the sea ice edge advancement from September to October and surface wind averaged over September–October was negligible ( $r = -0.01$ ), suggesting that surface winds play a minor role. The BT and NIC + MASIE exhibited similar features (figures omitted).

**Figure 3.** (a) Histograms of sea ice edge positions indicated for the rectangular box shown in Figure 2d based on NT over December–May (%; shaded), and the corresponding Hovmöller diagrams for December–May averages of (b) meridional wind at 10 m height ( $\text{m s}^{-1}$ ; positive for northward), (c) ocean temperature averaged over 0–300 m depth ( $^{\circ}\text{C}$ ; shaded), and (d) sea ice thickness (m; shaded) were obtained for the same rectangular box. The gray horizontal lines indicate 74.5°N (lower line) and 76.5°N (upper line). The black lines indicate the modes of the histograms in panel (a). The labels on the ordinate show the distance from the northern rim of the rectangular box ( $\times 100 \text{ km}$ ). The abscissa shows the year (e.g., 1980 corresponds to December 1979–May 1980).

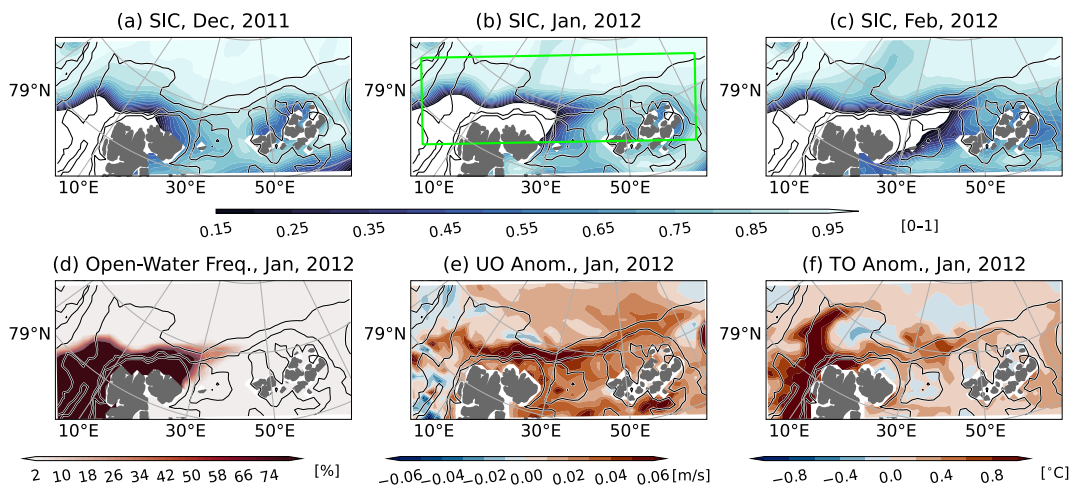


**Figure 5.** Horizontal maps of (a–c) monthly mean sea ice concentration (shaded) based on NT for December 2011, January 2012, and February 2012, respectively, and corresponding maps in January 2012 for (d) the percentages of days when sea ice concentration is below 15% (%), (e) surface zonal ocean current anomaly ( $\text{m s}^{-1}$ ), and (f) ocean temperature anomalies averaged for 0–300 m depth ( $^{\circ}\text{C}$ ). The anomalies are differences from the averages obtained from 1980 to 2023. The isolines of bathymetry for 200, 500, and 2,500 m are indicated with the contours. The green rectangular box in panel (b) is used to construct the time series shown in Figure 6a.

### 3.4. Sea Ice Edge Along the Continental Slope in January–March

High sea ice edge occurrences extended eastward along the continental slope in January in 2009–2023 compared with the previous periods (Figures 2d–f). The seasonal evolution in 2011/12 (Figure 5) typified this situation. The northern part of the Barents Sea had been covered by sea ice by December (Figure 5a). However, the open-water region in the north of Svalbard, which is known as “Whalers Bay” (Duarte et al., 2020), expanded eastward along the continental slope in January (Figure 5b), corresponding to the eastward extension of the sea ice edge. The open-water region expanded in February (Figure 5c) and diminished in March. The expansion of the open-water region accompanied local augmentation in the open-water day fraction (Figure 5d), eastward ocean current anomaly (Figure 5e), and ocean temperature anomaly (Figure 5f) in January and February (figure omitted).

The relationship between the expansion of the open-water region and the surrounding environment was further investigated. We quantified the extent of the open-water region every January (see Text S2 in Supporting Information S1) and constructed a time series (Figure 6a). Though the vertical axis in Figure 6a is limited to 0–1,000 km, the reference box is 1,300 km wide to encompass all the daily sea ice edges. The extent of the open-water region was typically 370 km in 1980–2004 but increased to 670 km in 2012 and onward.

We compared the composite maps of ocean currents and sea ice thickness in 2012–2023 and 1980–2004 to elucidate the decadal-scale change. The eastward current (Figure 6b) was significantly stronger along the continental slope, and the sea ice thickness (Figure 6c) was significantly thinner over the Barents Sea and the interior Arctic Ocean in 2012–2023 than in 1980–2004. These results suggest that stronger surface ocean currents and sea ice thinning have resulted in a large expansion of the open-water region in the recent decade.

Furthermore, the interannual variability was elucidated by evaluating the correlation between the open-water region extent in January (Figure 6a) and other fields. All variables were detrended by removing their linear least-squares fitting from 1980 to 2023. The results were insensitive to the detrending method. The simultaneous correlations with surface current, sea ice thickness, and sea ice concentration in January were statistically significant at the 90% confidence level over the Barents Sea (not shown). In addition, the lagged correlation with sea ice thickness (Figure 6d) and concentration (Figure 6e) in the preceding September was statistically significant. Thus, we speculated that the thinner sea ice and lower sea ice concentration in September were reflected in the sea ice properties in the following January, leading to the greater expansion of the open-water region because thinner sea ice with lower concentration should be easier to melt and be transported eastward by a narrow warm current. These relationships could be relevant for seasonal forecasting and should be verified by further investigation.

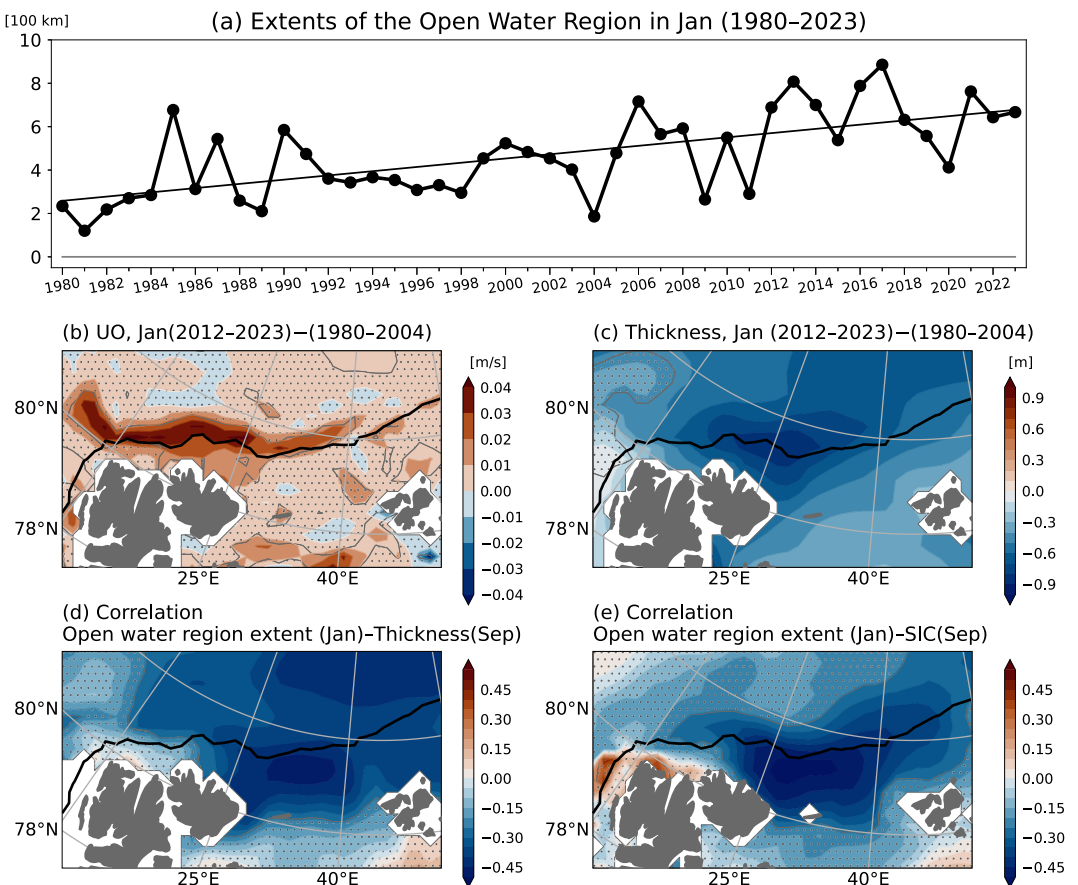


**Figure 6.** (a) Extent of the open-water region based on NT in January in the rectangular box shown in Figure 5b. See Text S2 in Supporting Information S1 for details. The thin line indicates the linear least-squares fitting line. Composite differences between averages for 2012–2023 and 1984–2004 in panel (b) surface zonal current speed ( $\text{m s}^{-1}$ ) and (c) sea ice thickness (meter). Correlation coefficients between the detrended open-water region extent in January and (d) sea ice thickness or (e) sea ice concentration in the preceding September. In panels (b–e), the hatching is applied where the differences or correlations are statistically insignificant at the 90% confidence level. The isolines of bathymetry for 500 m are indicated with the contours.

The sensitivity of these results for the selection of data sets was investigated by constructing the same time series based on BT and NIC + MASIE (Figure S4 in Supporting Information S1). All the time series were confirmed to yield similar results. Nevertheless, it is worth mentioning that the NT and BT exhibited systematically larger open-water regions than NIC + MASIE, likely originating from the underestimation of thin ice by passive microwave remote sensing (Ivanova et al., 2015).

#### 4. Variability in Sea Ice Edge Positions in the Greenland Sea

In the Greenland Sea, the East Greenland Current (EGC) flows southwestward along the continental slope (Figure 1c), transporting large amounts of sea ice from the Fram Strait (Spreen et al., 2020). To the east, the relatively warm Norwegian Atlantic Front Current flows northeastward along Mohns Ridge (Bosse & Fer, 2019).

##### 4.1. Seasonal Evolution and Long-Term Changes

Figure 7 shows sea ice edge occurrence maps for the Greenland Sea for each season. The sea ice edges were generally well anchored along the EGC throughout the year. However, the band of high occurrence along the EGC was less clear in July–September for 2009–2023 (Figure 7l) compared with the previous periods (Figures 7j and 7k), which is further addressed in the next subsection. It is also worth noting that sea ice edge occurrence in January–March was high along the Norwegian Atlantic Front Current in addition to along the EGC in 1980–1993

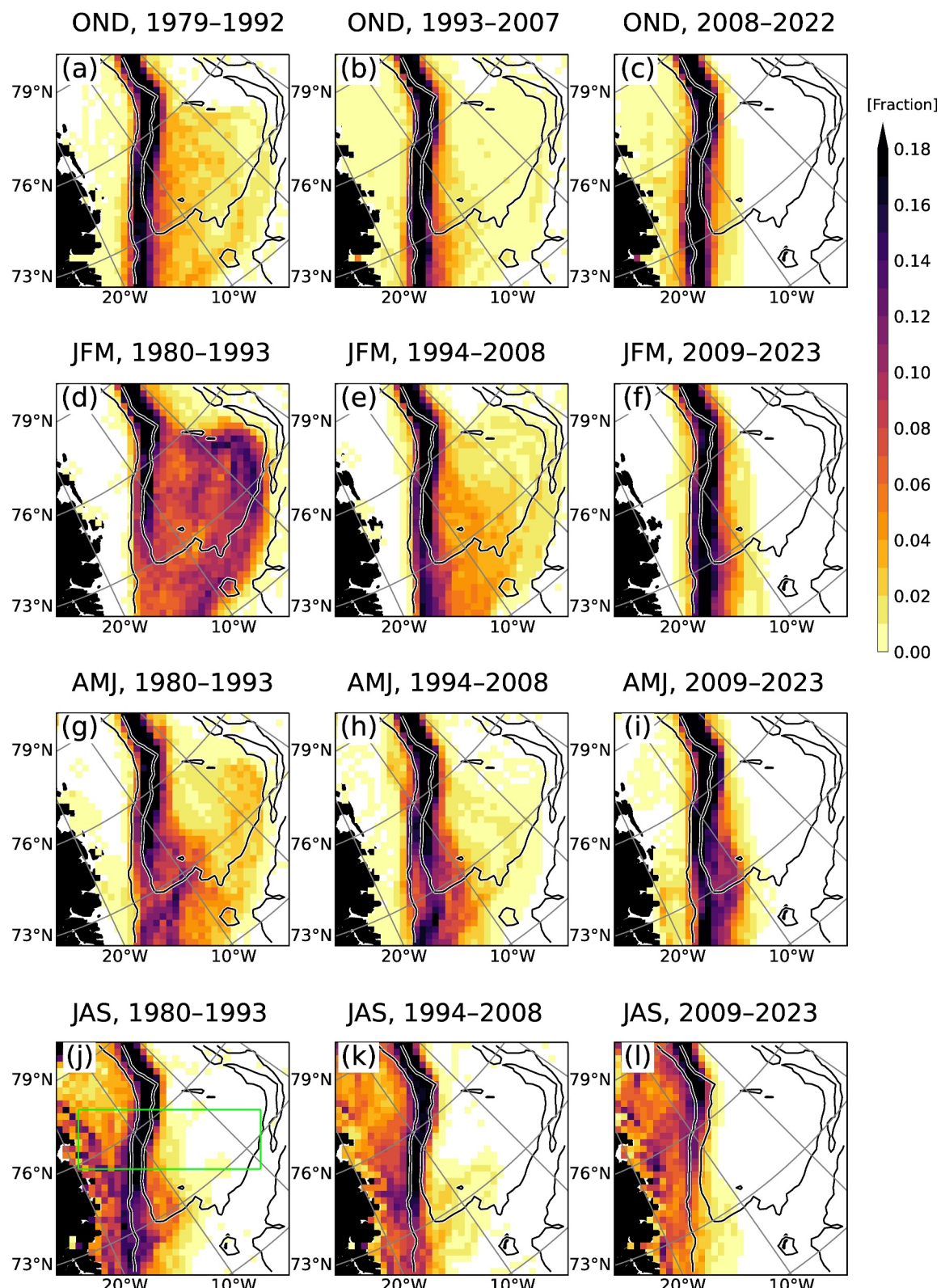


**Figure 7.** Sea ice edge occurrences at each grid cell based on NT accumulated over (a–c) October–December (d–f) January–March (g–i) April–June, and (j–l) July–September are constructed for the periods indicated on the top of each panel. The isolines of bathymetry for 500 and 2,500 m are indicated with the contours. The rectangular box in panel (j) indicates the target domain for constructing the sea ice edge position histograms shown in Figure 8.

(Figure 7d), which is the signature of the Odden ice tongue (Comiso et al., 2001; Germe et al., 2011; Rogers & Hung, 2008; Shuchman et al., 1998; Wadhams, 1981; Wadhams & Comiso, 1999). Meanwhile, the Odden ice tongue was rarely generated in the subsequent period (Figures 7e and 7f). The BT, NIC, and MASIE exhibited similar features (Figure S2 in Supporting Information S1 for JFM as a typical example).

The high sea ice edge occurrences along the EGC from October to April can be attributed to the warm Atlantic Water of the EGC, which inhibits sea ice expansion by sea ice transport crossing the EGC or heat loss from the open-water surface (figures omitted). The sea ice edges retreated slightly during May–June but remained close to the EGC throughout the analysis period. Thus, in the following section, the recent changes in sea ice edge positions in July–September are investigated in detail.

#### 4.2. Sea Ice Edge Variability From July to September

We constructed sea ice edge position histograms (Figure 8) estimated for the rectangular box shown in Figure 7j. The sea ice edge positions are the relative distance from the continental slope (i.e., locations with 500-m bathymetry). The positive value means that the sea ice edges are located on the offshore side. When a sea ice edge was missing because of the disappearance of the sea ice, the samples were neglected when constructing the histograms. The missing ratio of the sea ice edges is shown in the bar graphs in Figure 8. See Text S2 in Supporting Information S1 for the detailed method.

Until 1998, the sea ice edges in July were typically located on the offshore side of the continental slope (shaded in Figure 8a). However, they intruded into the continental shelf in 1999 and were frequently located on the continental shelf in the recent decade. Likewise, in August (not shown) and September (Figure 8c), the sea ice edges tended to be located around the continental slope until around 2006. However, they were frequently located on the continental shelf or had disappeared in the subsequent period (black bars in Figure 8d).

By constructing composites of sea ice properties, we elucidated how the sea ice edges were maintained near the continental slope until the mid-2000s. The composite maps were constructed with years when the modes of sea ice edge position histograms in September were located within 25 km from the continental slope or on the offshore side for the period from 1979 to 2006 (highlighted with the purple lines in Figure 8), hereafter referred to as “reference” years. Furthermore, to elucidate the recent sea ice edge position changes, we also constructed composite maps with years when the modes in September were located more than 25 km away from the continental slope or when the sea ice edges were missing more than 50% after 2006 (orange lines in Figure 8).

Figure 9a shows a composite map of the sea ice concentration in June for the reference years. The sea ice concentration amounted to 0.6 and more on the continental shelf. The seasonal decreases in sea ice concentration from June to July (Figure 9b) and July to August (not shown) were zonally uniform and modest (typically 0.2). The sea ice concentration increased from August to September (not shown). Thus, the sea ice concentration was maintained above the threshold (15%) over the entire continental shelf throughout the year, and hence the sea ice edges seasonally retreated only slightly. The small seasonal decrease in sea ice concentration can be likely attributed to the large sea ice thickness (Figure 9c) and large sea ice transport from the Fram Strait.

Figures 9d–9f show the composite maps of sea ice properties when the sea ice edges in September exhibited large retreats or were missing from 2007 to 2023. The sea ice concentration in June (Figure 9d) was lower than that of the reference years, with a 90% confidence level. Moreover, its seasonal decrease from June to July (Figure 9e) was considerably larger, consistent with the large sea ice edge retreat. The larger decrease was perhaps related to the thinner sea ice (Figure 9f; significantly thinner than the reference years with the 90% confidence level) and enhanced ice-albedo feedback due to the lower sea ice concentration in June. These characteristics are consistent with a recent decrease in sea ice thickness and transport from the Fram Strait (Sumata et al., 2022, 2023) and the recent warming of the EGC (de Steur et al., 2023). These aspects should be investigated quantitatively in future studies.

Lastly, we compared the sea ice edge positions based on the NT, BT, and NIC + MASIE. All the sea ice products represented the recent frequent intrusion of the sea ice edges into the continental shelf, and the frequent sea ice missing in September (Figure S5 in Supporting Information S1), and therefore these results are insensitive to data products. Nevertheless, some discrepancies are worth mentioning. The sea ice edge missing ratio in September was distinctly lower in the BT and NIC + MASIE than in the NT. Additionally, the MASIE occasionally exhibited modes near the continental slope in some years when the NT represented a large edge retreat. Our brief

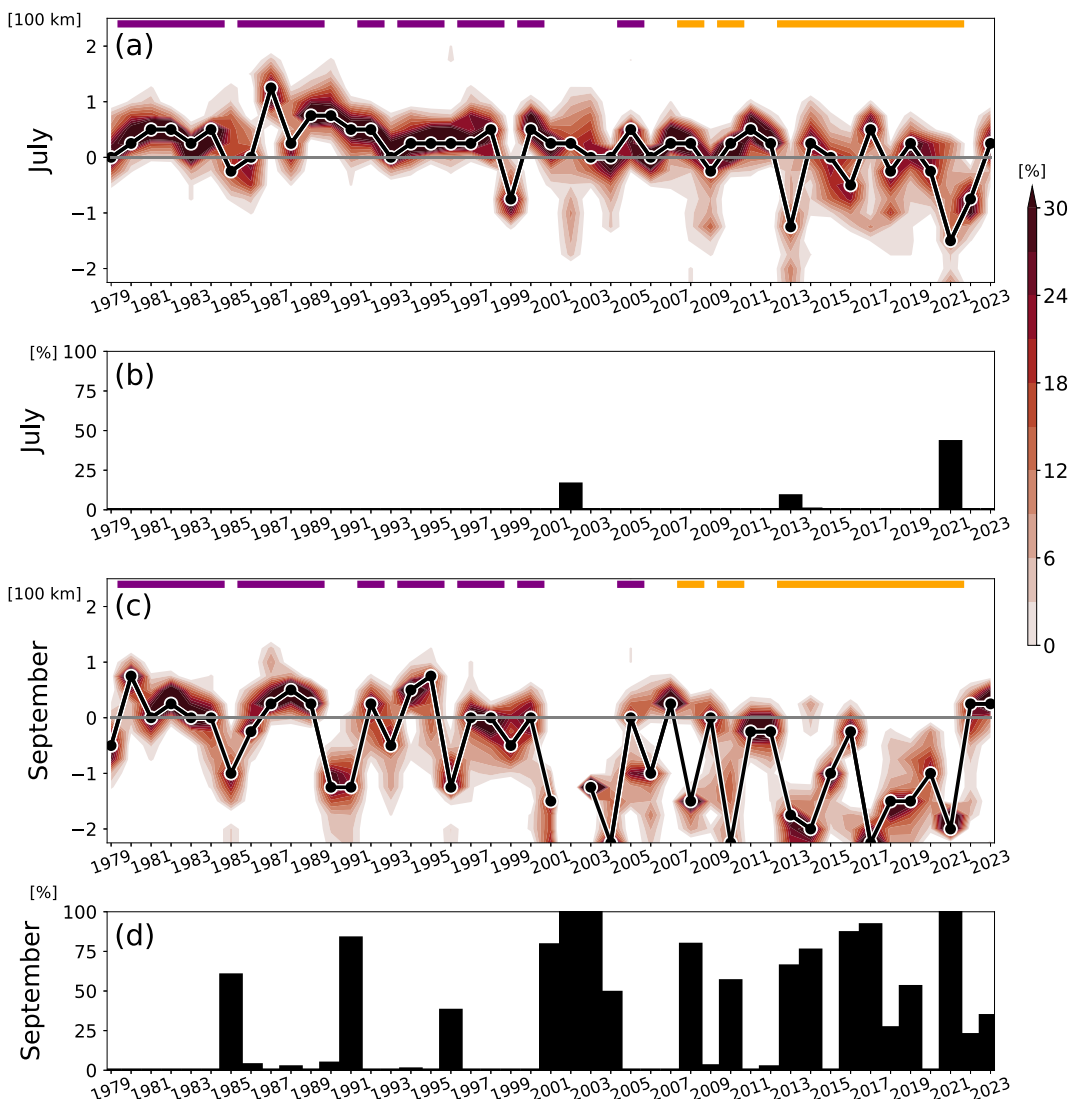


**Figure 8.** (a) Histograms of the sea ice edge positions based on NT in July measured as relative distances from the continental slope obtained for the rectangular box in Figure 7j and (b) the fractions of sea ice edges missing. See Text S2 in Supporting Information S1 for details. Panels (c, d) Same as in panels (a, b), respectively, but for September. The black lines indicate the modes of the histograms while they are omitted when the sea ice edge missing fraction is 100%. The color lines on the top indicate the classification of “reference” years (purple) and the years when sea ice edges exhibited large retreat or were frequently missing (orange).

investigation revealed that, even when the NT exhibited no ice, the BT retained sea ice near the coast of Greenland, and the MASIE represented sea ice near the EGC (Figure S6 in Supporting Information S1 for 24 September 2014 as an example). The discrepancies likely relate to the different filters for mitigating the land spillover (please refer to their user guide) and the underestimation of sea ice concentration in the NT and BT under thin ice and melt pond conditions (Comiso et al., 1997; Meier, 2005).

## 5. Discussion

Besides sea ice edge positions, we compared various data products for sea ice thickness, sea ice motion, atmosphere, and ocean fields, as listed in Table S1 of Supporting Information S1 for verification (see Text S1 in Supporting Information S1 for the description of the data sets). We confirmed that the main results were generally insensitive to the selection of data sets except for some minor quantitative differences. Nevertheless, the present results should be further verified because data reliability may be limited over sea ice regions.

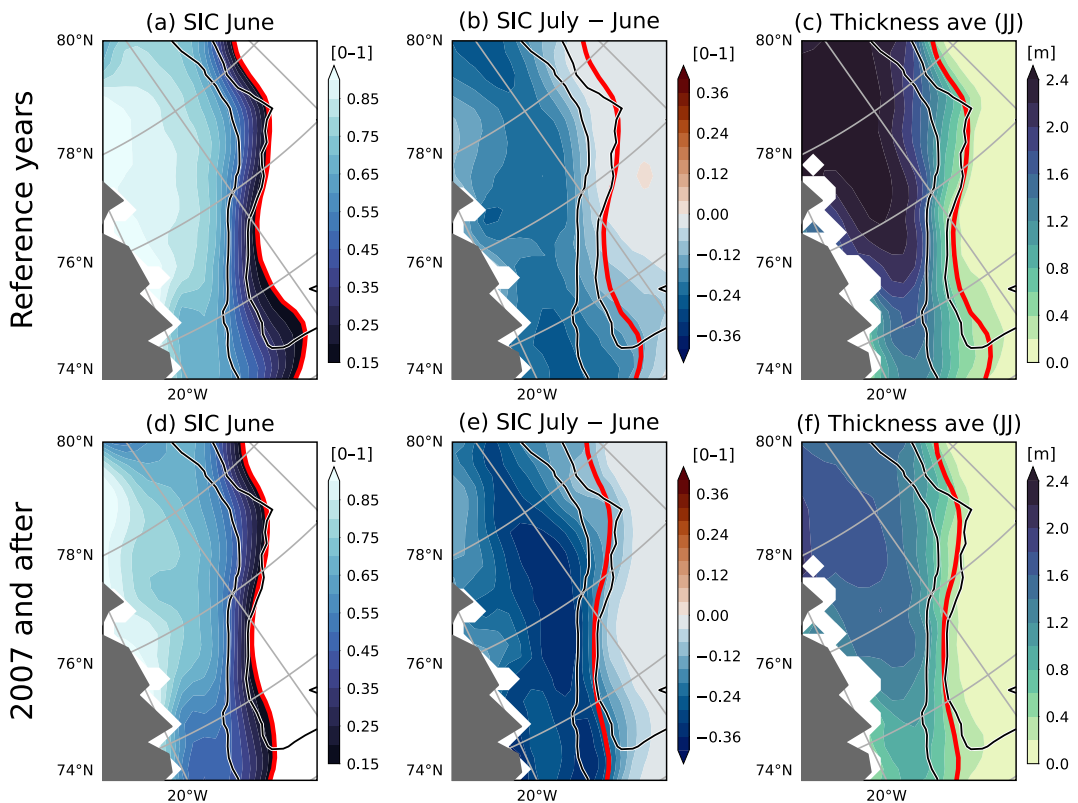


**Figure 9.** (a) Composite of sea ice concentration based on NT in June (shaded; the 15% contour is highlighted as a red line) constructed for the “reference” years, and (b) the corresponding difference between July and June (shaded). The red line in panel (b) indicates the 15% contour of the composited sea ice concentration averaged for June–July. (c) The corresponding composite of sea ice thickness (shaded) and sea ice concentration (red contour; only for 15%) averaged for June–July. The isolines of bathymetry for 500 and 2,500 m are indicated with the black contours. Panels (d–f) Same as in panels (a–c), respectively, but for the composites with the years when sea ice edges exhibited large retreat or were missing during 2007–2023, as highlighted with the orange lines in Figure 8.

As described in Appendix A, we tried to expand our analysis to include the period before 1979. However, the data availability and quality seemed insufficient for obtaining reliable results. Therefore, the present study did not address extensive longer-term analysis.

Atmosphere–ice–ocean interactions are particularly active near the sea ice edge. Recent changes in the typical sea ice edge positions may manifest as anomalous atmospheric and ocean circulation, for example, by inducing convection in the atmosphere (Kawai, 2021; Masunaga, 2024; Seo & Yang, 2013) and ocean (Våge et al., 2018). The sea ice edge statistics in the present study should be useful for addressing this topic in future studies.

## 6. Summary

The present study investigated the sea ice edge position over the Barents and Greenland Seas based on satellite-derived sea ice products from 1979 to 2023. In winter–spring in the Barents Sea, sea ice edges were close to narrow warm currents flowing in the central Barents Sea. Although the interannual variability was mostly regulated by surface winds until 2004, sea ice edges in the subsequent period were anchored along a narrow current between the GB and CB regardless of the wind direction. Sea ice edges were also frequently identified near the continental slope in the northern Barents Sea from 2008 to 2023, likely because the warm currents obstruct the seasonal sea ice edge advance and maintain the open-water region. In summer, sea ice edges were broadly distributed over the Barents Sea, and their geographical relationship to ocean currents was unclear. In the Greenland Sea, sea ice edges were maintained near the EGC year-round until 2006; thus, seasonality was indistinct. However, the sea ice edges in summer tended to retreat greatly in recent decades. These sea ice edge characteristics were verified using several sea ice products. Although the present study suggested that ocean

currents, surface wind direction, and sea ice thickness play an important role in determining sea ice edge positions and their recent changes, their relative roles should be quantitatively investigated in future work.

## Appendix A: A Long-Term Analysis Dating Back to Before 1979

We tried to extend our analysis to before 1979. See Text S1 in Supporting Information S1 for detailed descriptions of the data and data processing. The sea ice edge occurrence maps were constructed based on Ice Edge Positions in the Nordic Seas (Divine & Dick, 2007), which provided observed sea ice edge positions for each date during March–August over 1750–2002. The sea ice edge occurrence maps for 1750–1977 (Figure S7 in Supporting Information S1 for April and July) were similar to those obtained for 1980–2008 based on NT (Figures 2 and 7). Thus, the sea ice edge variability seems to remain unchanged from the 1750s until the 2000s. However, the reliability of this historical sea ice record was limited because the observations were very sparse and available once each year at most from 1750 to 1966.

Additionally, the Pan-Arctic Ice Ocean Modeling and Assimilation System forced with ERA-20C (PIOMAS-20C) (Schweiger et al., 2019) was used for this analysis, which was available continuously from 1901 to 2010. The sea ice edge exhibited virtually no temporal variation for some periods (e.g., 1991–1952 in January; Figure S8 in Supporting Information S1); this is likely because PIOMAS-20C assimilated the Met Office Hadley Center sea ice concentration and sea-surface temperature data set, which uses climatological-mean sea ice for much of the period to fill missing data (Titchner & Rayner, 2014). This example demonstrates that careful quality assessment would be required when using a sea ice product with long-term records dating to before 1979.

## Data Availability Statement

Sea ice products were obtained from NSIDC for the main data (DiGirolamo et al., 2022) (<https://doi.org/10.5067/MPYG15WAA4WX>), BT (Comiso, 2023) (<https://doi.org/10.5067/X5LG68MH013O>), NIC (U.S. National Ice Center et al., 2006) (<https://doi.org/10.7265/N5X34VDB>), MASIE (U.S. National Ice Center et al., 2010) (<https://doi.org/10.7265/N5GT5K3K>), and Ice Edge Positions in the Nordic Seas (Divine & Dick, 2007) (<https://doi.org/10.7265/N59884X1>). The sea ice motion data were obtained from NSIDC (Tschudi et al., 2019) (<https://doi.org/10.5067/INAUW07QH7B>) and Global Change Observation Mission in JAXA (Global Change Observation Mission, 2024) ([https://www.eorc.jaxa.jp/AMSR/datacatalog/cryosphere/index\\_en.html#sim](https://www.eorc.jaxa.jp/AMSR/datacatalog/cryosphere/index_en.html#sim)). The PIOMAS (Polar Science Center, 2003) and PIOMAS-20C products (Polar Science Center, 2019) were obtained from the Polar Science Center ([http://psc.apl.uw.edu/research/projects/arctic-sea-ice-volume-anomaly/data/model\\_grid](http://psc.apl.uw.edu/research/projects/arctic-sea-ice-volume-anomaly/data/model_grid) and <http://psc.apl.uw.edu/research/projects/piomas-20c>, respectively). The monthly mean products of ERA5 (Hersbach et al., 2019) and ORASS5 (Copernicus Climate Change Service & Climate Data Store, 2021) were obtained from the Climate Data Store (<https://doi.org/10.24381/cds.f17050d7> and <https://doi.org/10.24381/cds.67e8eeb7>, respectively). The ETOPO1 was obtained from the NOAA National Geophysical Data Center (NOAA National Geophysical Data Center, 2009) (<https://doi.org/10.7289/V5C8276M>). Global Ocean Physics Reanalysis (Mercator Ocean International, 2018) was obtained from E.U. Copernicus Marine Service (<https://doi.org/10.48670/moi-00024>). The J-OFURO3 was obtained from Data Integration and Analysis System (Tomita, 2020) (<https://doi.org/10.20783/DIAS.612>). The JRA55 was obtained from Research Data Archive at the National Center for Atmospheric Research (Japan Meteorological Agency/Japan, 2013) (<https://rda.ucar.edu/datasets/d628001>).

## Acknowledgments

We would like to thank the editors and three anonymous reviewers for their constructive comments, which greatly improved the original manuscript. This work was partially supported by the Arctic Challenge for Sustainability II (ArCS II) Project (Program Grant JPMXD1420318865) and the JSPS KAKENHI Grant (JP 22K20393). Some figures use the scientific color maps (Cramer, 2018) from <https://doi.org/10.5281/zenodo.1243862> and the CMOcean color maps (Thyng et al., 2016). We would like to thank Editage ([www.editione.jp](http://www.editione.jp)) for English language editing.

## References

- Amante, C., & Eakins, B. W. (2009). *ETOPO1 1 arc-minute global relief model: Procedures, data sources and analysis*. National Geophysical Data Center, NOAA. <https://doi.org/10.7289/V5C8276M>
- Årthun, M., Eldevik, T., Smedsrød, L. H., Skagseth, Ø., & Ingvaldsen, R. B. (2012). Quantifying the influence of Atlantic heat on Barents Sea ice variability and retreat. *Journal of Climate*, 25(13), 4736–4743. <https://doi.org/10.1175/JCLI-D-11-00466.1>
- Barton, B. I., Lenn, Y.-D., & Lique, C. (2018). Observed atlantification of the Barents Sea causes the polar front to limit the expansion of winter Sea Ice. *Journal of Physical Oceanography*, 48(8), 1849–1866. <https://doi.org/10.1175/JPO-D-18-0003.1>
- Bitz, C. M., Holland, M. M., Hunke, E. C., & Moritz, R. E. (2005). Maintenance of the Sea-Ice edge. *Journal of Climate*, 18(15), 2903–2921. <https://doi.org/10.1175/JCLI3428.1>
- Bosse, A., & Fer, I. (2019). Mean structure and seasonality of the Norwegian Atlantic front current along the Mohn ridge from repeated glider transects. *Geophysical Research Letters*, 46(22), 13170–13179. <https://doi.org/10.1029/2019gl084723>
- Cavalieri, D. J., Parkinson, C. L., Gloersen, P., & Jay Zwally, H. (1997). Arctic and Antarctic Sea Ice concentrations from multichannel passive-microwave satellite data sets: October 1978–September 1995 user's guide. Retrieved from <https://ntrs.nasa.gov/search.jsp?R=19980076134>

- Comiso, J. C. (2023). Bootstrap sea ice concentrations from nimbus-7 SMMR and DMSP SSM/I-SSMIS, version 4 [Dataset]. *NASA National Snow and Ice Data Center Distributed Active Archive Center*. <https://doi.org/10.5067/X5LG68MH0130>
- Comiso, J. C., Cavalieri, D. J., Parkinson, C. L., & Gloersen, P. (1997). Passive microwave algorithms for sea ice concentration: A comparison of two techniques. *Remote Sensing of Environment*, 60(3), 357–384. [https://doi.org/10.1016/S0034-4257\(96\)00220-9](https://doi.org/10.1016/S0034-4257(96)00220-9)
- Comiso, J. C., Wadhams, P., Pedersen, L. T., & Gersten, R. A. (2001). Seasonal and interannual variability of the Odden ice tongue and a study of environmental effects. *Journal of Geophysical Research*, 106(C5), 9093–9116. <https://doi.org/10.1029/2000jc000204>
- Copernicus Climate Change ServiceClimate, Data Store. (2021). ORASS global ocean reanalysis monthly data from 1958 to present [Dataset]. *Copernicus Climate Change Service (C3S) Climate Data Store (CDS)*. <https://doi.org/10.24381/CDS.67E8EEB7>
- Crameri, F. (2018). *Scientific colour maps: Perceptually uniform and colour-vision deficiency friendly*. Zenodo. <https://doi.org/10.5281/zenodo.1243862>
- de Steur, L., Sumata, H., Divine, D. V., Granskog, M. A., & Pavlova, O. (2023). Upper ocean warming and sea ice reduction in the East Greenland Current from 2003 to 2019. *Communications Earth & Environment*, 4(1), 1–11. <https://doi.org/10.1038/s43247-023-00913-3>
- DiGirolamo, N. E., Parkinson, C. L., Cavalieri, D. J., Gloersen, P., & Zwally, H. J. (2022). Sea ice concentrations from nimbus-7 SMMR and DMSP SSM/I-SSMIS passive microwave data, Version 2 [Dataset]. *NASA National Snow and Ice Data Center Distributed Active Archive Center*. <https://doi.org/10.5067/MPYG15WAA4WX>
- Divine, D. V., & Dick, C. (2006). Historical variability of sea ice edge position in the Nordic Seas. *Journal of Geophysical Research*, 111(C1). <https://doi.org/10.1029/2004JC002851>
- Divine, D. V., & Dick, C. (2007). March through August ice edge positions in the Nordic seas, 1750–2002, version 1 [Dataset]. *National Snow and Ice Data Center*. <https://doi.org/10.7265/N59884X1>
- Duarte, P., Sundfjord, A., Meyer, A., Hudson, S. R., Spreen, G., & Smedsrød, L. H. (2020). Warm Atlantic water explains observed sea ice melt rates north of Svalbard. *Journal of Geophysical Research, C: Oceans*, 125(8). <https://doi.org/10.1029/2019jc015662>
- Dukhovskoy, D. S., Ubnoske, J., Blanchard-Wrigglesworth, E., Hiester, H. R., & Proshutinsky, A. (2015). Skill metrics for evaluation and comparison of sea ice models. *Journal of Geophysical Research, C: Oceans*, 120(9), 5910–5931. <https://doi.org/10.1002/2015jc010989>
- Dumont, D. (2022). Marginal ice zone dynamics: History, definitions and research perspectives. *Philosophical Transactions. Series A, Mathematical, Physical, and Engineering Sciences*, 380(2235), 20210253. <https://doi.org/10.1098/rsta.2021.0253>
- Eriksen, E., Gjosæter, H., Prozorkevich, D., Shamray, E., Dolgov, A., Skern-Mauritzen, M., et al. (2018). From single species surveys towards monitoring of the Barents Sea ecosystem. *Progress in Oceanography*, 166, 4–14. <https://doi.org/10.1016/j.pocean.2017.09.007>
- Germe, A., Houssais, M.-N., Herbaut, C., & Cassou, C. (2011). Greenland Sea ice variability over 1979–2007 and its link to the surface atmosphere. *Journal of Geophysical Research*, 116(C10), C10034. <https://doi.org/10.1029/2011jc006960>
- Global Change Observation Mission. (2024). AMSR2/AMSR-E research products [Dataset]. *GCOM-W Research Product Distribution Service*. Retrieved from [https://suzaku.eorc.jaxa.jp/GCOM\\_W/research/resdist.html](https://suzaku.eorc.jaxa.jp/GCOM_W/research/resdist.html)
- Hersbach, H., Bell, B., Berrisford, P., Biavati, G., Horányi, A., Muñoz Sabater, J., et al. (2019). ERA5 monthly averaged data on single levels from 1940 to present [Dataset]. *Copernicus Climate Change Service (C3S) Climate Data Store (CDS)*. <https://doi.org/10.24381/CDS.F17050D7>
- Hersbach, H., Bell, B., Berrisford, P., Hirahara, S., Horányi, A., Muñoz-Sabater, J., et al. (2020). The ERA5 global reanalysis. *Quarterly Journal of the Royal Meteorological Society*, 146(730), 1999–2049. <https://doi.org/10.1002/qj.3803>
- Hoskins, B. J., & Valdes, P. J. (1990). On the existence of storm-tracks. *Journal of the Atmospheric Sciences*, 47(15), 1854–1864. [https://doi.org/10.1175/1520-0469\(1990\)047<1854:OTEOST>2.0.CO;2](https://doi.org/10.1175/1520-0469(1990)047<1854:OTEOST>2.0.CO;2)
- Inoue, J., Hori, M. E., & Takaya, K. (2012). The role of Barents Sea Ice in the wintertime cyclone track and emergence of a warm-arctic cold-Siberian anomaly. *Journal of Climate*, 25(7), 2561–2568. <https://doi.org/10.1175/JCLI-D-11-00449.1>
- Ivanova, N., Pedersen, L. T., Tonboe, R. T., Kern, S., Heygster, G., Lavergne, T., et al. (2015). Inter-comparison and evaluation of sea ice algorithms: Towards further identification of challenges and optimal approach using passive microwave observations. *The Cryosphere*, 9(5), 1797–1817. <https://doi.org/10.5194/tc-9-1797-2015>
- Japan Meteorological Agency/Japan. (2013). JRA-55: Japanese 55-year reanalysis, monthly means and variances [Dataset]. *Research Data Archive at the National Center for Atmospheric Research, Computational and Information Systems Laboratory*. <https://doi.org/10.5065/D60G3H5B>
- Kawai, Y. (2021). Low-level atmospheric responses to the sea surface temperature fronts in the Chukchi and Bering seas. *Frontiers in Marine Science*, 8. <https://doi.org/10.3389/fmars.2021.598981>
- Kolstad, E. W. (2006). A new climatology of favourable conditions for reverse-shear polar lows. *Tellus. Series A, Dynamic Meteorology and Oceanography*, 58(3), 344–354. <https://doi.org/10.1111/j.1600-0870.2006.00171.x>
- Kolstad, E. W. (2011). A global climatology of favourable conditions for polar lows. *Quarterly Journal of the Royal Meteorological Society*, 137(660), 1749–1761. <https://doi.org/10.1002/qj.888>
- Landgren, O. A., Seierstad, I. A., & Iversen, T. (2019). Projected future changes in marine cold-air outbreaks associated with polar lows in the northern North-Atlantic ocean. *Climate Dynamics*, 53(5), 2573–2585. <https://doi.org/10.1007/s00382-019-04642-2>
- Masunaga, R. (2024). Near-surface wind convergence along the Sea Ice edge in the Greenland Sea: Its mean state and shaping process. *Journal of Geophysical Research*, 129(16), 2864–2889. <https://doi.org/10.1029/2024JD040888>
- Meier, W. N. (2005). Comparison of passive microwave ice concentration algorithm retrievals with AVHRR imagery in Arctic peripheral seas. *IEEE Transactions on Geoscience and Remote Sensing: A Publication of the IEEE Geoscience and Remote Sensing Society*, 43(6), 1324–1337. <https://doi.org/10.1109/TGRS.2005.846151>
- Meier, W. N., Fetterer, F., Stewart, J. S., & Helfrich, S. (2015). How do sea-ice concentrations from operational data compare with passive microwave estimates? Implications for improved model evaluations and forecasting. *Annals of Glaciology*, 56(69), 332–340. <https://doi.org/10.3189/2015oga69a694>
- Melsom, A., Palmer, C., & Müller, M. (2019). Validation metrics for ice edge position forecasts. *Ocean Science*, 15(3), 615–630. <https://doi.org/10.5194/os-15-615-2019>
- Mercator Ocean International. (2018). Global ocean physics reanalysis [Dataset]. *E.U. Copernicus Marine Service*. <https://doi.org/10.48670/moi-00021>
- NOAA National Geophysical Data Center. (2009). ETOPO1 1 Arc-Minute global Relief model [Dataset]. *NOAA National Centers for Environmental Information*. Retrieved from <https://www.ngdc.noaa.gov/metadata/geoportal/rest/metadata/item/gov.noaa.ngdc.mgg.dem:316/html>
- Nøst, O. A., & Isachsen, P. E. (2003). The large-scale time-mean ocean circulation in the Nordic Seas and Arctic Ocean estimated from simplified dynamics. *Journal of Marine Research*, 61(2), 175–210. <https://doi.org/10.1357/002224003322005069>
- Papritz, L., & Spengler, T. (2017). A Lagrangian climatology of wintertime cold air outbreaks in the irrminger and nordic seas and their role in shaping air-sea heat fluxes. *Journal of Climate*, 30(8), 2717–2737. <https://doi.org/10.1175/JCLI-D-16-0605.1>

- Polar Science Center. (2003). PIOMAS variables on model grid [Dataset]. *Polar Science Center*. Retrieved from [https://psc.apl.uw.edu/research/projects/arctic-sea-ice-volume-anomaly/data/model\\_grid](https://psc.apl.uw.edu/research/projects/arctic-sea-ice-volume-anomaly/data/model_grid)
- Polar Science Center. (2019). PIOMAS-20C Sea Ice thickness reconstruction [Dataset]. *Polar Science Center*. Retrieved from <https://psc.apl.uw.edu/research/projects/piomas-20c/>
- Rogers, J. C., & Hung, M.-P. (2008). The Odden ice feature of the Greenland Sea and its association with atmospheric pressure, wind, and surface flux variability from reanalyses. *Geophysical Research Letters*, 35(8). <https://doi.org/10.1029/2007gl032938>
- Schweiger, A. J., Wood, K. R., & Zhang, J. (2019). Arctic Sea ice volume variability over 1901–2010: A model-based reconstruction. *Journal of Climate*, 32(15), 4731–4752. <https://doi.org/10.1175/JCLI-D-19-0008.1>
- Seo, H., & Yang, J. (2013). Dynamical response of the Arctic atmospheric boundary layer process to uncertainties in sea-ice concentration. *Journal of Geophysical Research*, 118(22), 12–383. <https://doi.org/10.1002/2013jd020312>
- Serreze, M. C., Holland, M. M., & Stroeve, J. (2007). Perspectives on the Arctic's shrinking sea-ice cover. *Science*, 315(5818), 1533–1536. <https://doi.org/10.1126/science.1139426>
- Shuchman, R. A., Josberger, E. G., Russel, C. A., Fischer, K. W., Johannessen, O. M., Johannessen, J., & Gloersen, P. (1998). Greenland Sea Odden sea ice feature: Intra-annual and interannual variability. *Journal of Geophysical Research*, 103(C6), 12709–12724. <https://doi.org/10.1029/98jc00375>
- Skagseth, Ø., Eldevik, T., Årthun, M., Asbjørnsen, H., Lien, V. S., & Smedsrød, L. H. (2020). Reduced efficiency of the Barents Sea cooling machine. *Nature Climate Change*, 10(7), 661–666. <https://doi.org/10.1038/s41558-020-0772-6>
- Spensberger, C., & Spengler, T. (2021). Sensitivity of air-sea heat exchange in cold-air outbreaks to model resolution and sea-ice distribution. *Journal of Geophysical Research*, 126(5). <https://doi.org/10.1029/2020jd033610>
- Spreen, G., Steur, L., Divine, D., Gerland, S., Hansen, E., & Kwok, R. (2020). Arctic sea ice volume export through Fram strait from 1992 to 2014. *Journal of Geophysical Research: C: Oceans*, 125(6). <https://doi.org/10.1029/2019jc016039>
- Stroeve, J. C., Serreze, M. C., Holland, M. M., Kay, J. E., Malanik, J., & Barrett, A. P. (2012). The Arctic's rapidly shrinking sea ice cover: A research synthesis. *Climatic Change*, 110(3), 1005–1027. <https://doi.org/10.1007/s10584-011-0101-1>
- Sumata, H., de Steur, L., Divine, D. V., Granskog, M. A., & Gerland, S. (2023). Regime shift in Arctic Ocean sea ice thickness. *Nature*, 615(7952), 443–449. <https://doi.org/10.1038/s41586-022-05686-x>
- Sumata, H., de Steur, L., Gerland, S., Divine, D. V., & Pavlova, O. (2022). Unprecedented decline of Arctic sea ice outflow in 2018. *Nature Communications*, 13(1), 1747. <https://doi.org/10.1038/s41467-022-29470-7>
- Thyng, K. M., Greene, C. A., Hetland, R. D., Zimmerle, H. M., & DiMarco, S. F. (2016). True colors of oceanography: Guidelines for effective and accurate colormap selection. *Oceanography*, 29(3), 9–13. <https://doi.org/10.5670/oceanog.2016.66>
- Titchner, H. A., & Rayner, N. A. (2014). The Met Office Hadley Centre sea ice and sea surface temperature data set, version 2: 1. Sea ice concentrations. *Journal of Geophysical Research*, 119(6), 2864–2889. <https://doi.org/10.1002/2013jd020316>
- Tomita, H. (2020). J-OFURO3 [Dataset]. *Data Integration and Analysis System (DIAS)*. <https://doi.org/10.20783/DIAS.612>
- Tschudi, M., Meier, W. N., & Stewart, J. S. (2020). An enhancement to sea ice motion and age products at the National Snow and Ice Data Center (NSIDC). *The Cryosphere*, 14(5), 1519–1536. <https://doi.org/10.5194/tc-14-1519-2020>
- Tschudi, M., Meier, W. N., Stewart, J. S., Fowler, C., & Maslanik, J. (2019). Polar pathfinder daily 25 km EASE-grid sea ice motion vectors, Version 4 [Dataset]. *NASA National Snow and Ice Data Center Distributed Active Archive Center*. <https://doi.org/10.5067/INAUWU07QH7B>
- U.S. National Ice Center, Fetterer, F., & Fowler, C. (2006). U.S. National ice center arctic Sea Ice Charts and climatologies in gridded format, 1972 - 2007, version 1 [Dataset]. *National Snow and Ice Data Center*. <https://doi.org/10.7265/N5X34VDB>
- U.S. National Ice Center, Fetterer, F., Savoie, M., Helfrich, S., & Clemente-Colón, P. (2010). Multisensor analyzed Sea Ice extent - northern hemisphere (MASIE-NH), version 1 [Dataset]. *National Snow and Ice Data Center*. <https://doi.org/10.7265/N5GT5K3K>
- Våge, K., Papritz, L., Håvik, L., Spall, M. A., & Moore, G. W. K. (2018). Ocean convection linked to the recent ice edge retreat along east Greenland. *Nature Communications*, 9(1), 1287. <https://doi.org/10.1038/s41467-018-03468-6>
- Wadhams, P. (1981). The ice cover in the Greenland and Norwegian seas. *Reviews of Geophysics*, 19(3), 345–393. <https://doi.org/10.1029/rg019i003p00345>
- Wadhams, P., & Comiso, J. C. (1999). Two modes of appearance of the Odden ice tongue in the Greenland sea. *Geophysical Research Letters*, 26(16), 2497–2500. <https://doi.org/10.1029/1999gl900502>
- Xia, W. T., Xie, H. J., & Ke, C. Q. (2014). Assessing trend and variation of Arctic sea-ice extent during 1979–2012 from a latitude perspective of ice edge. *Polar Research*, 33(1), 21249. <https://doi.org/10.3402/polar.v33.21249>

## References From the Supporting Information

- Brodzik, M. J., & Knowles, K. W. (2002). EASE-grid- A versatile set of equal-area projections and grids. In M. F. Goodchild & A. J. Kimerling (Eds.), *Discrete global grids: A web book* (pp. 98–113). Retrieved from <https://escholarship.org/uc/item/9492q6sm>
- Drévillon, M., Fernandez, E., & Lelloouche, J. M. (2023). *Product user manual for the global ocean physical multi year product*. E.U. Copernicus Marine Service. Retrieved from <https://catalogue.marine.copernicus.eu/documents/PUM/CMEMS-GLO-PUM-001-030.pdf>
- Harada, Y., Kamahori, H., Kobayashi, C., Endo, H., Kobayashi, S., Ota, Y., et al. (2016). The JRA-55 reanalysis: Representation of atmospheric circulation and climate variability. *Journal of the Meteorological Society of Japan. Ser. II*, 94(3), 269–302. <https://doi.org/10.2151/jmsj.2016-015>
- Hersbach, H., Bell, B., Berrisford, P., Biavati, G., Horányi, A., Muñoz Sabater, J., et al. (2018). ERA5 hourly data on single levels from 1940 to present [Dataset]. *Copernicus Climate Change Service (C3S) Climate Data Store (CDS)*. <https://doi.org/10.24381/cds.adbb2d47>
- Kobayashi, S., Ota, Y., Harada, Y., Ebata, A., Moriya, M., Onoda, H., et al. (2015). The JRA-55 reanalysis: General specifications and basic characteristics. *Journal of the Meteorological Society of Japan. Ser. II*, 93(1), 5–48. <https://doi.org/10.2151/jmsj.2015-001>
- Schweiger, A. J., Lindsay, R., Zhang, J., Steele, M., Stern, H., & Kwok, R. (2011). Uncertainty in modeled Arctic sea ice volume. *Journal of Geophysical Research*, 116(C8), C00D06. <https://doi.org/10.1029/2011JC007084>
- Shimada, K., Kamoshida, T., Itoh, M., Nishino, S., Carmack, E., McLaughlin, F., et al. (2006). Pacific Ocean inflow: Influence on catastrophic reduction of sea ice cover in the Arctic Ocean. *Geophysical Research Letters*, 33(8). <https://doi.org/10.1029/2005gl025624>
- Tomita, H., Hihara, T., Kako, S., Kubota, M., & Kutsuwada, K. (2019). An introduction to J-OFURO3, a third-generation Japanese ocean flux data set using remote-sensing observations. *Journal of Oceanography*, 75(2), 171–194. <https://doi.org/10.1007/s10872-018-0493-x>

- Yoshizawa, E., Kamoshida, T., & Shimada, K. (2022). Sea ice motion vector retrievals from AMSR2 89-GHz data: Validation algorithm with simultaneous multichannel observations. *Journal of Atmospheric and Oceanic Technology*, 40(1), 3–13. <https://doi.org/10.1175/JTECH-D-22-0049.1>
- Zhang, J., & Rothrock, D. A. (2003). Modeling global Sea Ice with a thickness and enthalpy distribution model in generalized curvilinear coordinates. *Monthly Weather Review*, 131(5), 845–861. [https://doi.org/10.1175/1520-0493\(2003\)131<845:MGSIWA>2.0.CO;2](https://doi.org/10.1175/1520-0493(2003)131<845:MGSIWA>2.0.CO;2)
- Zuo, H., Balmaseda, M. A., Tietsche, S., Mogensen, K., & Mayer, M. (2019). The ECMWF operational ensemble reanalysis–analysis system for ocean and sea ice: A description of the system and assessment. *Ocean Science*, 15(3), 779–808. <https://doi.org/10.5194/os-15-779-2019>